JOURNAL OF PROPULSION AND POWER
Vol. 25, No. 2, March–April 2009

Spray Structure in Near-Injector Region of Aerated Jet in Subsonic Crossflow

J. Lee* and K. A. Sallam†
Oklahoma State University, Stillwater, Oklahoma 74078
K.-C. Lin‡
Taitech, Inc., Beavercreek, Ohio 45433
and
C. D. Carter§
U.S. Air Force Research Laboratory, Wright–Patterson Air Force Base, Ohio 45433

DOI: 10.2514/1.36719

An experimental study of the breakup of an aerated liquid jet in subsonic crossflow was carried out. Digital double-pulsed holographic microscopy was used, employing a double exposure charge-coupled device sensor. The measurements include droplet locations, sizes and sphericity, and three-dimensional velocities. Droplet velocities in three dimensions were measured by tracking their displacements in the streamwise and cross-stream direction and by tracking the change in the plane of focus in the spanwise direction. The study demonstrated that digital holographic microscopy was suitable for probing the nonspherical droplets in the near-injector region. The droplet size distributions followed Simmons's universal root-normal distribution and thus could be fully described by the Sauter mean diameter alone. The distributions of the streamwise and cross-stream velocities were uniform in the near-injector region and could be characterized by the mass-average velocity except for very small and very large droplets.

Nomenclature

d	=	drop diameter
d_0	=	injector orifice diameter
M	=	freestream Mach number
N	=	number of pixels
q_0	=	jet/freestream momentum flux ratio, $\rho_L^2 v_j^2 / \rho_\infty^2 u_\infty^2$
U_∞	=	freestream velocity
u	=	velocity component in the cross-stream (horizontal) direction
v	=	velocity component in the jet streamwise (vertical) direction
v_j	=	jet exit velocity
w	=	velocity component in the spanwise (normal to the page) direction
x	=	cross-stream (horizontal) distance from the injector exit
y	=	streamwise (vertical) distance from the injector exit
z	=	spanwise (normal to the page) distance from the injector exit
Δx	=	pixel size
$\Delta\xi$	=	hologram resolution
λ	=	wavelength
ν	=	kinematic viscosity
ρ	=	density
σ	=	surface tension

Subscripts

G	=	aerating gas property
j	=	jet exit property
L	=	liquid property
∞	=	freestream property

Superscript

$\sim$	=	mass-averaged properties

Presented as Paper 1043 at the 46th AIAA Aerospace Sciences Meeting and Exhibit, Reno, Nevada, 7–10 January 2008; received 17 January 2008; revision received 21 October 2008; accepted for publication 21 October 2008.

*Graduate Student, Mechanical and Aerospace Engineering.
†Assistant Professor, Mechanical and Aerospace Engineering; khaled.sallam@okstate.edu. Senior Member AIAA (Corresponding Author).
‡Senior Research Scientist. Associate Fellow AIAA.
§Principal Aerospace Engineer. Associate Fellow AIAA.

I. Introduction

A GOOD understanding of the phenomena of liquid jet breakup is essential for a successful design of gas turbine fuel injectors, ramjet and scramjet engines, diesel fuel injectors, medical sprays, and inkjet printers, among others. The major objective of most injectors is to atomize a liquid jet into a fine spray. Pressure atomizers, such as a plain orifice nozzle injector, accomplish this objective by using a very small orifice diameter and/or a very high injection pressure. In many applications this solution is not feasible, because small orifice diameters tend to get clogged easily and high injection pressures are not always available. Aerated liquid injectors (also known as effervescent atomizers), on the other hand, can easily provide dense sprays of fine droplets with low injection pressures and large orifice diameter by introducing gas bubbles into the liquid stream inside the injector. Aerated injection is similar to the flash atomization because it produces gas bubbles inside the injector for promoting atomization. However, unlike flash atomizers, aerated injection can easily control the amount of bubbles and their sizes without the complications of dissolving gas or heating the liquid to its boiling point. The aerated liquid injector allows a large exit orifice diameter because atomization quality depends on liquid sheet thickness rather than the orifice diameter. Moreover, the aerated atomization generates a fine spray at low injection pressures and low gas flow rates for a wide range of operating viscosities.

The dense-spray region near the injector is optically opaque for phase Doppler interferometry, for example, phase Doppler particle analyzers (PDPA). Moreover, two-dimensional imaging methods,

for example, shadowgraphy, have a limited depth of field that renders them impractical for measuring droplet sizes and velocities of three-dimensional spray structure. Kim and Lee [1] studied the two-phase internal flow pattern inside the aerated injector for different aerating gas-to-liquid mass flow rate ratios (GLR) by using a transparent aerated injector and pulsed shadowgraphy. The flow patterns inside the aerated injector could be classified into three regimes as follows: bubbly flow regime, intermittent flow regime, and annular flow regime. When the GLR is small, the flow pattern inside the injector becomes bubbly because small bubbles are distributed throughout the liquid. However, at a large value of GLR, a liquid layer is formed along the wall of the injector exit passage and the internal flow pattern becomes annular. At the intermediate GLR, the internal flow pattern randomly wanders between the bubbly flow and annular flow regimes.

Lefebvre et al. [2] investigated the influences of the nozzle geometric design on the atomization performance. They concluded that the exit orifice diameter has little effect on the mean droplet sizes. Buckner and Sojka [3] investigated effervescent atomization of high viscosity fluids in the annular flow regime. They concluded that the mean droplet diameter is sensitive to GLR but nearly is independent of the liquid viscosity, the fluid supply pressure, and the mixture mass flow rate. Lund et al. [4] reported on the influence of surface tension on effervescent atomization. They found that the drop sizes decreased with the increase of the surface tension.

Santangelo and Sojka [5] investigated the near nozzle spray structure of an effervescent atomizer using focused image holography. They divided the spray structure into three flow regimes based on GLR. In the bubbly flow regime, GLR $< 2\%$, the breakup process is governed by the expansion of individual bubbles. A cylinder of liquid (a trunk) breaks up into ligaments and droplets due to individual bubble expansion. In the transition flow regime, the trunk became distorted and was replaced by a ring of limbs, which formed a tree. In the annular flow regime, the trunk is greatly reduced in length, and a small number of large limbs break up into a higher number of thinner limbs and branches. Sutherland et al. [6] reported on the entrainment of ambient air into the spray produced by a ligament controlled effervescent atomizer. Their results showed that the surface tension had a negligible effect on the normalized entrainment, whereas increasing the liquid viscosity from 0.001 to 0.02 Pa $\cdot$ s resulted in an increase in normalized entrainment by 30–50%. They report that the entrainment number, which was a function of the steady entrainment rate and the momentum rate, was relatively insensitive to liquid physical properties but increased with GLR. Wade et al. [7] reported on the spray characteristics of an effervescent atomizer operating in the MPa injection pressure ranges. They found that the Sauter mean diameter (SMD) decreases with the increase in injection pressure. They also reported the SMD decreased with an increase in exit orifice diameter which was not expected and in contrast to earlier results [2]. The spray cone angle was not influenced by the exit orifice diameter but increased with the increase of GLR and the injection pressure.

Lin et al. [8,9] studied the spray structure of the aerated liquid jet in crossflow using PDPA and pulsed shadowgraphy. They reported that as the GLR increased, the droplet distribution in the spray plume changed from multidispersed to monodispersed. They also suggested a correlation for the penetration height of the aerated liquid jet injected in the crossflow. Sallam et al. [10] investigated the primary breakup of round aerated liquid jets in supersonic crossflow using single- and double-pulsed shadowgraphy and holography. For GLR greater than 2%, the aerated liquid jet was in the annular flow regime, and the spray cone angle and surface breakup properties upstream and downstream of the liquid sheet were similar indicating a weak aerodynamic effect. They developed a correlation for the aerated liquid sheet thickness.

Miller et al. [11] successfully used digital holography to probe the droplet sizes of aerated liquid jet in crossflow at downstream distances between $x/d_0 = 25$ and $x/d_0 = 50$ using a single laser beam. They used two methods, digital inline holography and digital holographic microscopy (DHM) (also known as digital microscopy holography), and demonstrated that the two methods are suitable for measuring the properties of the dense-spray region and insensitive to the nonspherical droplets. They concluded that DHM is the best method for providing valuable information about the small droplets encountered in the spray because of its ability to resolve very small details. Miller et al. [11] used two injector exit diameters of 1 and 5 mm, GLR of 4 and 8%, and jet-to-freestream momentum ratios of 0.74 and 4 to investigate the spray structure at two locations of 25 and 50 jet diameters. The increase in GLR from 4 to 8% reduced the SMD perhaps due to the squeezing effect of the liquid sheet. The variation of the exit diameters influenced the number of droplets produced but not the droplet sizes. The jet-to-freestream momentum flux ratio had an effect on controlling the spray plume penetration. At the same GLR, the SMD was reduced between two different downstream locations of $x/d_0 = 25$ and $x/d_0 = 50$. They suggested that this effect was due to the secondary breakup. They did not perform, however, any velocity measurements and therefore could not measure the Weber number of the droplets in the near-injector region.

Despite the recent advances reported in the literature, there is still a lack of data on droplet sizes and velocities in the near-injector region of aerated jets in crossflow (i.e., $x/d_0 < 25$). Velocimetry and size diagnostics for droplets in the near-injector region are needed to fill this gap. The present study demonstrates the applicability of digital holographic diagnostics to provide these measurements in the challenging near-injector region and provides velocities and size distributions of effervescent atomization in subsonic crossflow.

II. Experimental Method

A. Apparatus

The aerated liquid jet breakup experiments were performed in a subsonic wind tunnel with a test section of 0.3 m (height)$\times$ 0.3 m (width) $\times$ 0.6 m (length). This test section had float glass side walls and floor, and an acrylic ceiling to provide optical access. The range of air velocities was from 3 to 60 m/s at normal temperature and pressure. The wind-tunnel's contraction ratio was 16:1, and the velocity inside the test section had a variation within $\pm 1\%$ of the mean freestream velocity. Air velocities in the wind tunnel could be measured within $\pm 2\%$. The test liquid was supplied from a cylindrical chamber (constructed of type 304 stainless steel) having a diameter of 100 mm and a height of 300 mm, and the aerating gas for mixing with the liquid was provided from a pressure tank with a volume of 0.18 m^3 and an air pressure limit up to 5000 kPa. The aerated injector was installed on the acrylic ceiling of the test section to provide optical access. The exit diameter (d_0) of the aerated liquid injector used for this research was 1.0 mm. Aerating gas supplied from the storage tank comes in to meet with the liquid inside the nozzle by traveling through the outer tube and passing through 100 μm holes as shown in Fig. 1. The jet forms an

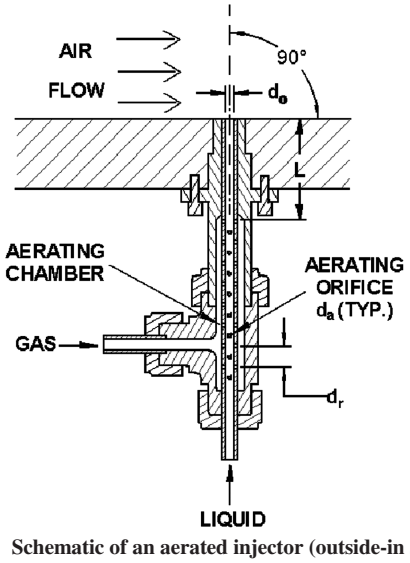

Fig. 1 Schematic of an aerated injector (outside-in setup).

annular-type two-phase flow composed of a gas core surrounded by a thin liquid sheet at sufficient GLR (the value of GLR at which the injector delivers an annular flow is design dependent). Air pressurized to 1.1 MPa was used as the aerating gas and water pressurized to 1.1 MPa was used as the liquid.

The schematic diagram of the experimental apparatus including optical setup is shown in Fig. 2. The volumetric flow rates of the liquid and the aerating gas were controlled by rotameters. The reading error of the air flow rate was within ± 3 cm^3/s, and that of the water flow meter was within ± 0.02 cm^3/s. To maintain a GLR of 8%, an airflow rate of 100 cm^3/s and a water flow rate of 145 cm^3/s were used. The uncertainty in the gas flow rate measurement is 3% and the uncertainty in the liquid flow rate measurement is 1%. An aluminum breadboard was installed under the wind-tunnel test section for easy routing of the double-pulsed lasers from an optical table to the wind-tunnel test section. Moreover, this breadboard has a rail that can be moved horizontally. This was used to transverse the charge-coupled device (CCD) camera and the objective lens and the spatial filter assembly with 1 mm accuracy. The schematic of the double-pulsed inline digital holographic microscopy is shown in Fig. 3. To create a hologram one needs a reference wave and an objective wave. However, the two waves can be within the same expanding laser beam as shown in Fig. 3 where the portion of the laser beam which was unaffected by the object can be used as the reference wave. The pulse duration needs to be short because the displacement of the droplet during the exposure can cause significant loss in the quality of the hologram. The exposure duration sets the highest limit for the droplet velocity that can be measured. The holograms were captured on a cooled interline transfer double exposure CCD camera (PCO 2000) having 2048×2048 pixels. For double-pulsing capability, two laser pulses were synchronized with the double exposure time of CCD by a delay generator. Two frequency doubled Nd:YAG lasers (Spectra Physics Model LAB-150, 532 nm wavelength, 7 ns pulse duration, and up to 300 mJ/pulse) that could be fired with a pulse separation as small as 100 ns were used as the light source. The two laser beams were aligned with a polarized beam combiner, and their intensities were controlled by a half-wave plate and a beam dump as shown in Fig. 3. A photodetector and an oscilloscope (Lecroy model 9314L) were used to measure the separation time between the two pulses. An objective lens (M 5×) and a 15 μm pinhole were used to expand the laser beam for digital holographic microscopy. The distance from the light source to the CCD was recorded within 1 mm accuracy during the test because it is needed for the digital reconstruction process. The resolution of the digital hologram depends on the distance from the object to the CCD, the wavelength of the light, and the pixel size of the CCD. The resolution of the hologram was determined by Schnars and Jueptner [12] as follows:

$$\Delta\xi = \lambda d / N \Delta x \tag{1}$$

where $\Delta\xi$ is the resolution, λ is the wavelength, d is the recording distance, that is, the distance from the object to the CCD, N is the number of pixels, and Δx is the pixel size. The distance between the objective lens and the aerated jet was minimized for good resolution, and the distance between the aerated jet and the CCD sensor was minimized for a good field of view. The total distance between the objective lens and the CCD sensor was 550 mm.

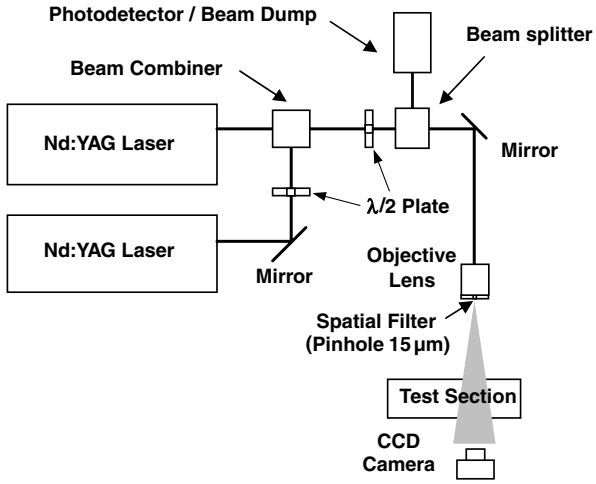

Fig. 3 Optical setup for DHM.

B. Instrumentation and Measuring Technique

When the digital hologram is stored on the CCD sensor, it can easily be reconstructed by a numerical algorithm [12]. After the reconstruction process, three-dimensional volume information is expressed by many reconstruction holograms focused on each two-dimensional plane. Because of the expanding laser beam used for DHM, the spatial calibration is continuously changing for each one of these two-dimensional planes. To conduct the spatial calibration, one needs at least three pins placed at three different distances from the CCD sensor. In the present study, four pins with the same diameter ($d_{\text{pin}} = 0.5$ mm) as shown in Fig. 4 were used to spatially calibrate the reconstructed holograms. The spacing among four pins was, respectively, 5 mm in the spanwise direction, that is, the laser beam direction. The hologram for spatial calibration was obtained with a distance of 550 mm between the objective lens and the CCD, and the Q-switch laser energy used was 52.8 mJ/pulse.

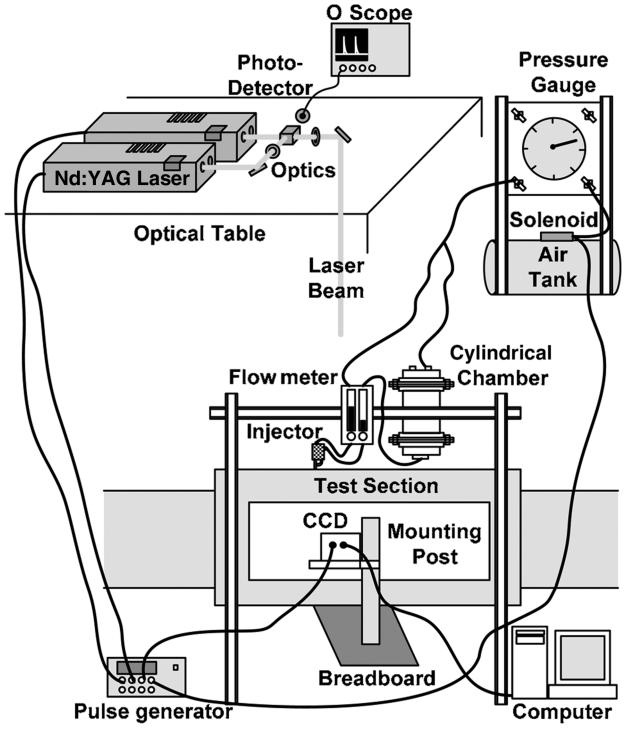

Fig. 2 Experimental apparatus.

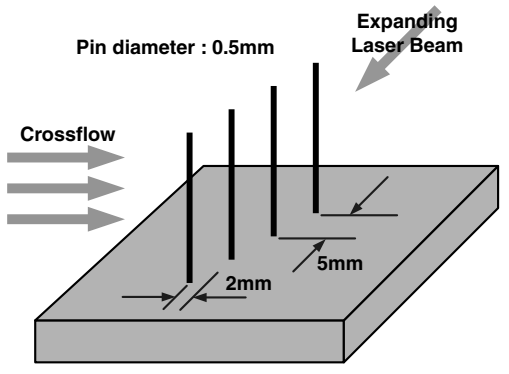

Fig. 4 Schematic of four pins for spatial calibration.

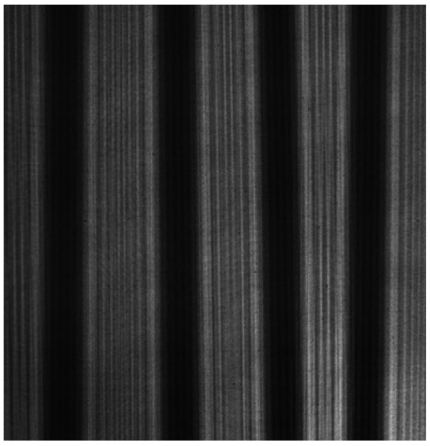

a)

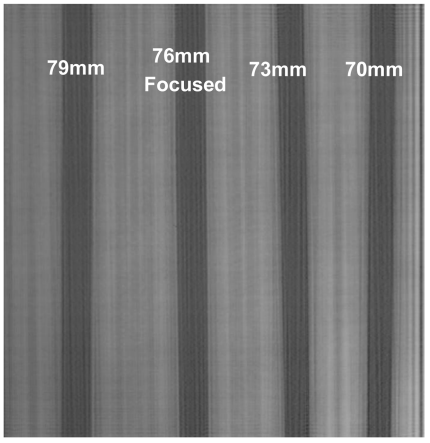

b)

Fig. 5 Hologram a) recorded for spatial calibration and b) reconstructed at the spanwise depth of 76 mm from the CCD sensor.

Figure 5a shows the original hologram of four pins and reconstructed two-dimensional image at the depth of 76 mm. When the image of a pin is focused on a two-dimensional plane, the others are out of focus. The second pin in Fig. 5b is very focused, but the other pins are out of focus because this hologram was reconstructed at the depth of 76 mm. Four pins have been consecutively reconstructed with a 3-mm distance interval ranging from 70 to 79 mm as shown in Fig. 6. In other words, the actual distance (the spacing of four pins) is 5 mm, but each pin was reconstructed with a distance interval of 3 mm. The spanwise actual distance was determined by this ratio. Because of the expanding laser beam diameter, the reconstructed image of each of the identical four pins had a different diameter. The spatial calibration relationship used in the present study is shown in Fig. 6. The linear correlation of Fig. 6 is as follows:

$$Y = -0.0213X + 5.5914 \tag{2}$$

where Y is the ratio of actual pin diameter to reconstructed pin diameter (mm/pixel) and X is the reconstruction distance (mm). The streamwise (vertical) actual distance and cross-stream (horizontal) actual distance can be calibrated with this equation by counting the pixel number for all reconstructed holograms. Thus, this equation becomes very useful for calculating the actual distance in each reconstructed two-dimensional plane.

The smallest droplets with diameters of 12 μm were measured with uncertainties of 73%. The smallest SMD of 40 μm was measured with uncertainty of 22%. The uncertainty in locating the droplet position in the spanwise direction (and hence the spanwise droplet velocities) depends on how well the droplet plane of focus can be found. Because reconstructions were made with 0.17 mm increments in the spanwise direction, the location of the centroid of the droplet can be known within $\pm$0.17 mm. The time interval

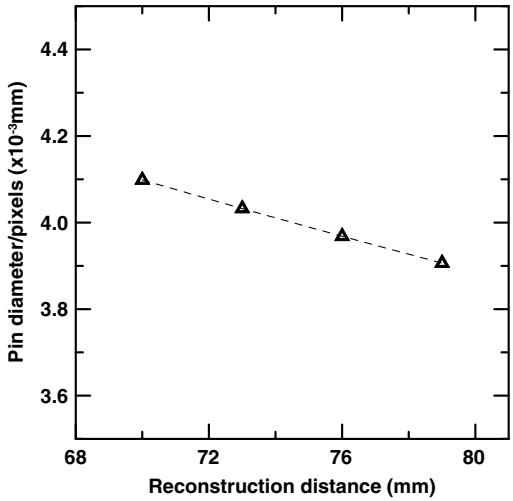

Fig. 6 Spatial calibration between actual distance and pixel numbers for all reconstruction distances within the field of view.

between the two laser pulses was controlled by a delay generator. An oscilloscope and a photodetector were used to measure the time interval between the double pulses. The uncertainties in the droplet velocities in the cross-stream and streamwise directions were less than 10% mainly due to sampling limitation. The location of the camera could be determined within $\pm$1 mm.

C. Test Condition

The test conditions are summarized in Table 1. The aerated injector had an exit diameter of 1 mm and it was tested at GLR of 8%. This gas–liquid mass flow rate ratio (GLR) was chosen to ensure an annular flow regime within the injector passage typical of practical fuel injectors. The momentum flux ratio was then selected based the required GLR and the limitations of the testing facility. To maintain a GLR of 8%, a water flow rate of 1.45 cc/s and an airflow rate of 103 cc/s were used. The injection pressure of 1.1 MPa was used for the aerating gas and the test liquid. City water was used as the test liquid (density = 999 kg/m^3, surface tension = 0.007 N/m, and kinematic viscosity = 1.12×10^{-6} m^2/s). To hold the jet-to-free-stream momentum flux ratio (q_0) at 0.74, the wind tunnel was set to a speed of $u_\infty = 61$ m/s. The freestream Mach number (M) was 0.18.

The digital holograms were recorded at a range of $x/d_0 = 0$–22.5 and $y/d_0 = 0$–27 with a field of view of each hologram of 9 × 9 mm. To overcome this limited field of view, the region of $x/d_0 = 0$–22.5 and $y/d_0 = 0$–27 was divided into nine investigation windows. Double-pulsed holograms were recorded for each window with the double exposure CCD sensor. Droplet diameters, locations, and three-dimensional velocities were measured in these nine investigation windows. The holograms were recorded starting at the top of the test section and then by moving the CCD sensor and the objective lens down in 9 mm increments. The CCD sensor continued to be lowered until no more droplets appeared.

After the holograms were digitally recorded, they were reconstructed at spanwise distances at increments of $\pm$0.17 mm throughout the spray volume. The reconstruction range was determined such that it could cover all the droplets in the spray at that particular location. The maximum range of reconstruction depth of spanwise direction was $\pm$13 mm. In each of the reconstructed

Table 1 Test conditions

d_0, mm	1.0
M, –	0.18
q_0, –	0.74
GLR, %	8
x/d_0, –	0–22.5
y/d_0, –	0–27
z/d_0, –	−13–13

holograms the focused images of the droplets were used to measure droplet diameters, locations, and three-dimensional velocities. The SMD was then calculated by averaging the droplet diameters over five spanwise incremental distances equaling 0.83 mm.

III. Results and Discussion

Double-pulsed DHM was used for probing the dense-spray near-injector region of the aerated liquid jet in crossflow. For the flow visualization of the dense-spray region, the spray structure map has been constructed by patching six high resolution holograms reconstructed at the same spanwise distance (away from the camera). Droplet sizes and three-dimensional velocities could be expressed together on the same plot.

A. Flow Visualization

A pulsed shadowgraph of aerated liquid jet in subsonic crossflow is shown in Fig. 7 for the present test conditions given in Table 1. Despite the high resolution achieved by using large format (127×127 mm) film, this shadowgraph has limited depth of field, typical of large magnification shadowgraphy. The shadowgraph projects a three-dimensional spray structure into two-dimensional spray with many drops out of focus due to the limited depth of field. To overcome the limited depth of field, DHM was used for the visualization. A standard resolution target (USAF 1951) was used to determine the spatial resolution of the present setup. Three bar patterns as small as 5 μm were successfully resolved using the present setup. Holograms digitally recorded on the CCD sensor have complete three-dimensional information. With the digital reconstruction process, three-dimensional information can be easily expressed with many two-dimensional slices. Thus, the entire flowfield for any spanwise distance could be investigated by numerical reconstruction of the original holograms. An original (recorded) hologram and a reconstructed hologram focused at the injector center plane are shown in Fig. 8. The entire spray structure of the dense-spray region of $x/d_0 < 13.5$ could be visualized with six high resolution holograms reconstructed at the same spanwise distance (depth) as shown in Fig. 9. The aerated jet was bent due to the crossflow.

B. Jet Surface Velocity

Liquid surface velocities near the injector exit were small due to the effect of a no-slip condition between the liquid and the injector wall. Farther away from the injector exit, the liquid surface velocity increases rapidly in the streamwise direction and then approaches a constant value. Streamwise mean liquid surface velocities, v_s, were measured using double-pulsed holograms as the function of the streamwise distances as shown in Fig. 10. The surface velocities increase within the streamwise location of $y/d_0 = 1.5$–5.5 and then become nearly constant as the jet approaches the location of $y/d_0 = 5.5$. A liquid surface velocity obtained at $y/d_0 = 6$ approached the mean jet velocity.

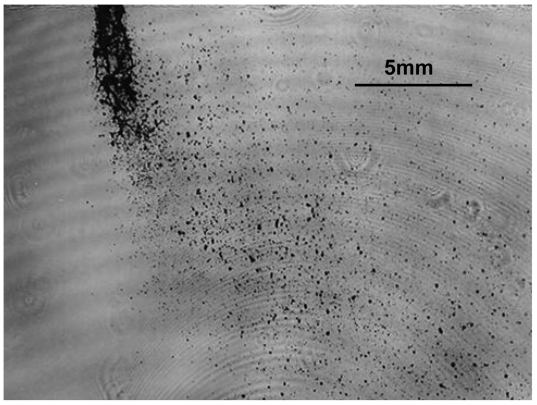

Fig. 7 Pulsed shadowgraph of aerated liquid jet in subsonic crossflow (test condition: 1-mm jet diameter, 8% GLR, and $q_0 = 0.74$).

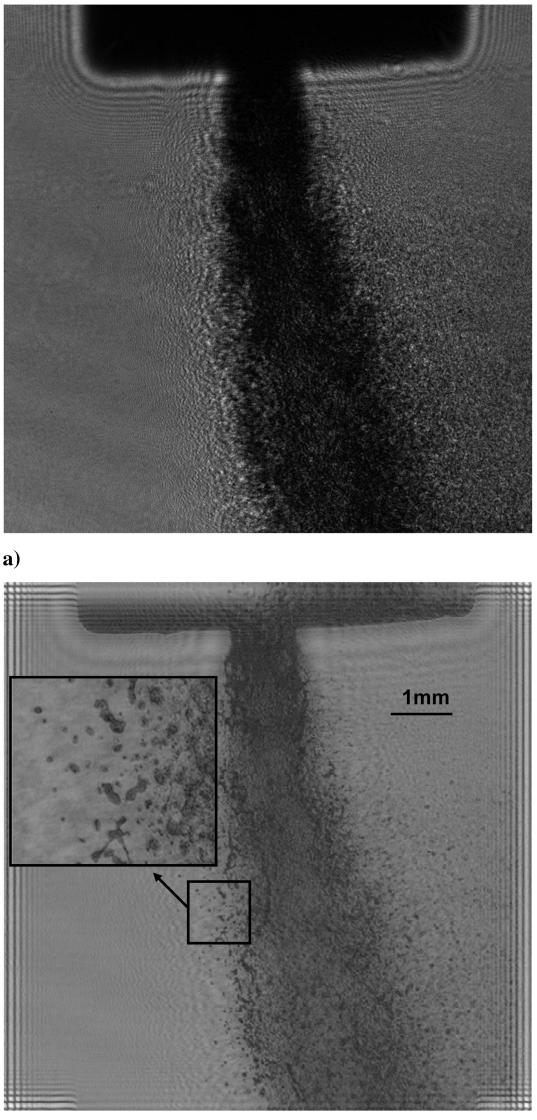

Fig. 8 Hologram a) recorded at the location of $x/d_0 = -4.5$–4.5 and $y/d_0 = 0$–9 (test conditions: 1-mm jet exit diameter, 8% GLR, and $q_0 = 0.74$) and b) reconstructed at the spanwise depth of 72 mm from the CCD sensor; the inset shows an enlarged image of the small rectangular region.

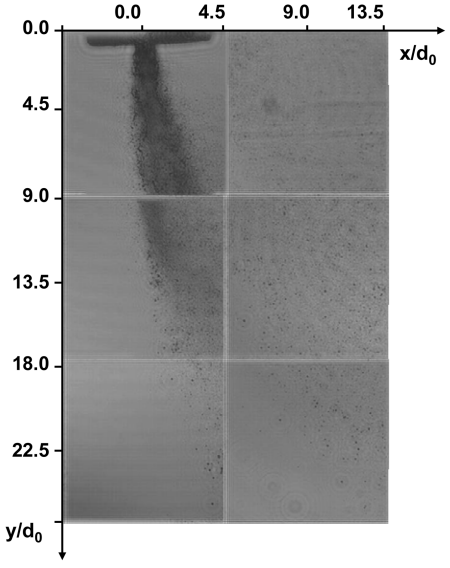

Fig. 9 Aerated liquid jet spray structure near injector region.

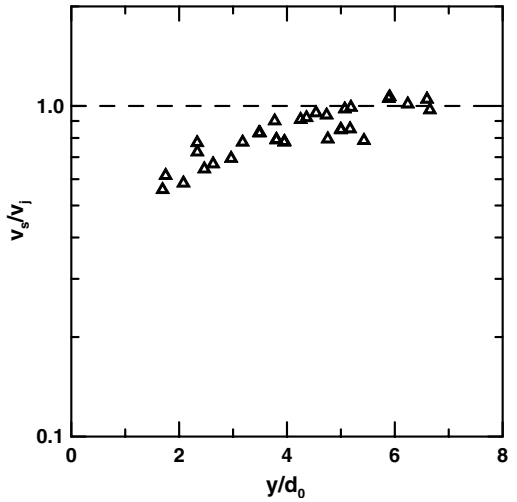

Fig. 10 Variation of surface velocity of the liquid sheet column ejected from the injector exit for the streamwise distance.

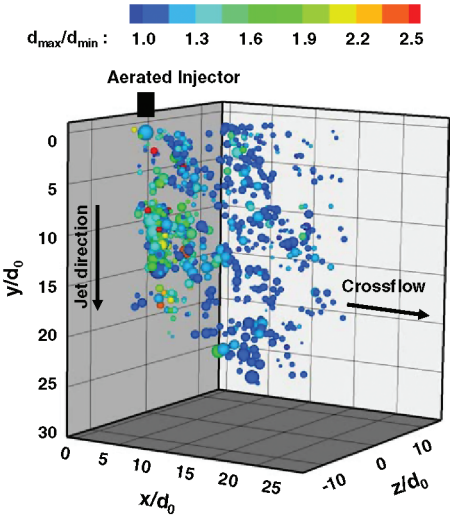

Fig. 12 Sphericity of individual droplets very near injector.

C. Drop Sizes

The spatial resolution of the current setup was 5 μm which allowed the size measurement of most droplets in the dense-spray region. Droplet sizes together with three-dimensional velocities were plotted as a function of the x–y–z location as shown in Fig. 11. Most droplets detached from the liquid column of the aerated jet were nonspherical. This explains why diagnostics such as PDPA are not successful in probing the near-injector region of the aerated liquid jets. These droplets were approximated as elliptical droplets, and their sizes were expressed by equivalent spherical diameters as follows:

$$d_{eq} = (d_{max} \times d_{min})^{1/2} \tag{3}$$

where d_{max} and d_{min} are the major axis and the minor axis for an elliptical droplet, respectively. The sphericity for all droplets in the near-injector region could be expressed by dividing the major axis by the minor axis as shown in Fig. 12. The average d_{max}/d_{min} for the present test conditions was 1.2. The droplets in the near-injector region were mainly nonspherical which makes them inaccessible for techniques such as PDPA. The droplets become spherical farther downstream from the injector due to the surface tension effects. The SMD decreased with the increase in downstream distance as shown in Fig. 13. The reduction of the SMD in the downstream region resulted from the secondary breakup. The SMD increased farther away from the injector center plane due to the annular spray structure of the aerated liquid jet.

Droplet sizes normalized by their mass median diameter (MMD) satisfy Simmons's universal root-normal distribution [13] with MMD/SMD = 1.2 as shown in Fig. 14. Therefore, the drop size distribution of aerated liquid jets in crossflow can be fully described by the SMD alone. The present results (for $0 < x/d < 25$, GLR = 8%) and previous results of Miller et al. [11] (for $x/d = 25$ and 50, GLR = 4% and 8%) are shown in Fig. 14. The majority of these points fall on the line where the MMD/SMD = 1.2. This agreement helps to validate the present experimental method.

D. Droplet Velocities

The droplet velocities in the streamwise and the cross-stream directions were measured by observing the displacement of the center of each droplet between the double pulses. The spanwise velocity could be measured by observing the change of the plane of focus of each drop measured between the double pulses. A typical double-pulsed reconstructed hologram used for measuring the three-dimensional velocities is shown in Fig. 15 for a pulse separation of 47 μs, $x/d_0 = 4.5$–13.5, and $y/d_0 = 18$–27. Three individual droplets marked with three capital letters A, B, and C are shown on two holograms corresponding to two time instants reconstructed at two different spanwise distances in Fig. 15. The droplet marked with the letter C and the letter C′ were focused at two different spanwise

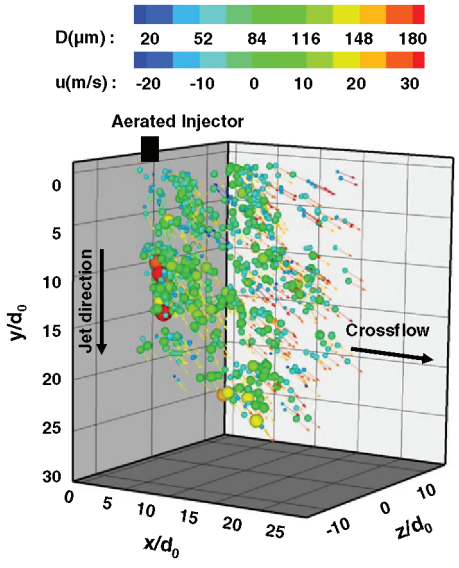

Fig. 11 Drop size distribution and three-dimensional velocities near injector region.

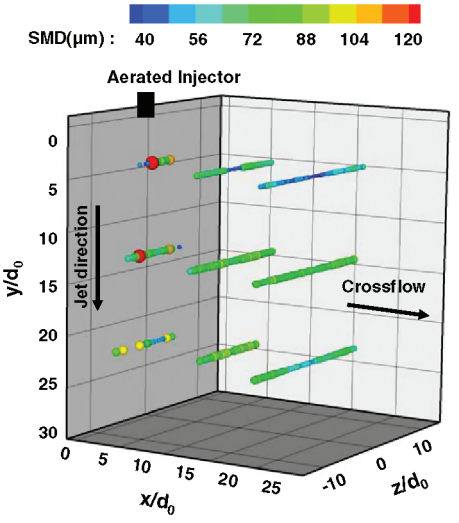

Fig. 13 Sauter mean diameter (SMD) distribution near injector.

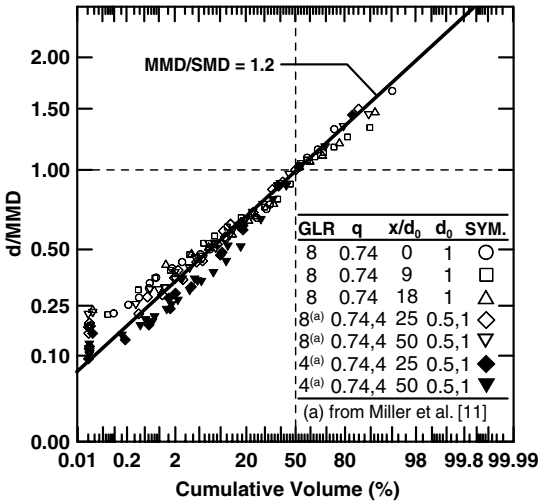

Fig. 14 Droplet size distribution plotted on a root-normal scale.

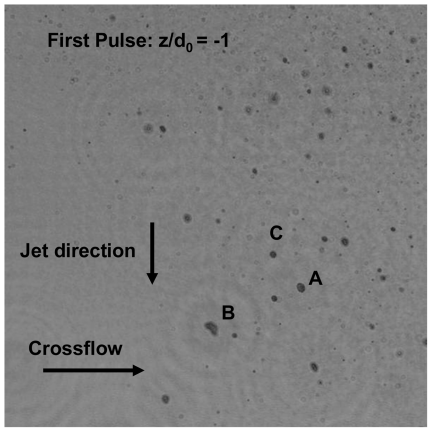

a)

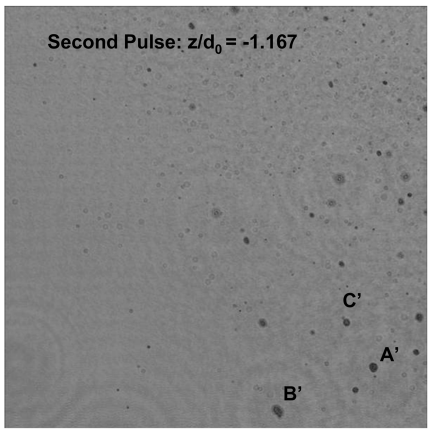

b)

Fig. 15 Double-pulsed reconstructed hologram at a) $t = 0$ and b) $t = 47$ μs. Test condition are GLR = 8%, $q_0 = 0.74$ at $x/d_0 = 9$, and $y/d_0 = 22$. The letters A, B, and C refer to distinct droplets that are tacked between the two pulses to yield velocity information.

depths of $z/d_0 = -1$ on the first hologram and $z/d_0 = -1.167$ on the second hologram. The droplet spanwise velocity was obtained by measuring the spanwise distance between the two focused planes and the time interval between the double pulses. The droplet marked with C has negative spanwise velocity, because the droplet has receded from the injector center plane between the double pulses. This is plausible because the liquid sheet of the aerated jet with hollow-type structure spreads toward both positive and negative directions away from the injector center plane. The measurements of the three-dimensional velocities were performed for all individual droplets in the nine investigation windows of the near-injector region.

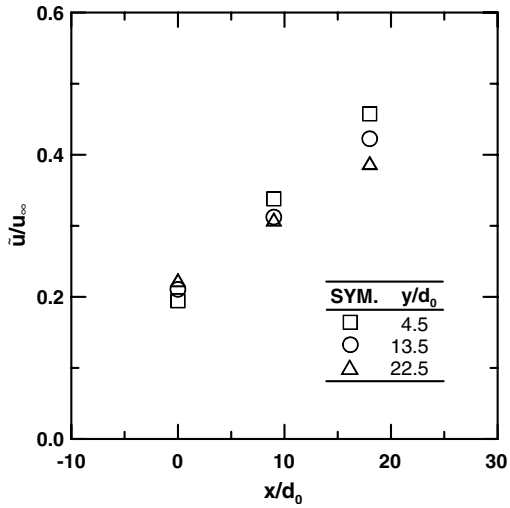

Fig. 16 Mass-averaged cross-stream droplet velocities for different x/d_0 locations.

Mass-averaged velocities in the streamwise and cross-stream directions, $\tilde{u}$ and $\tilde{v}$, have been measured within the spanwise distance of $z/d_0 = -13$–13. The mass-averaged cross-stream velocities normalized by the free crossflow velocity, $\tilde{u}/u_\infty$, are shown in Fig. 16. The mass-averaged cross-stream velocities increase with downstream distance due to the interaction between the gaseous crossflow and the droplets, and approach the crossflow velocity, u_∞, farther away from the injector. The mass-averaged streamwise velocities normalized by the mean aerated liquid jet velocity $\tilde{v}/v_j$ are shown in Fig. 17. The mass-averaged streamwise velocities decrease farther away from the injector exit.

The cross-stream droplet velocities distribution as a function of the droplet sizes is shown in Fig. 18. The cross-stream droplet velocities, u, were normalized by the mass-averaged cross-stream velocity, $\tilde{u}$, and droplet sizes were normalized by the SMD. The cross-stream velocities of smaller droplets are higher than the mass-averaged cross-stream velocity, and the cross-stream velocities of bigger droplets are lower than the mass-averaged velocity. This can be attributed to the effect of the mass of each droplet. The relationship between the cross-stream velocities normalized by the mass-averaged cross-stream velocity and the droplet sizes normalized by the SMD is expressed as follows:

$$u/\tilde{u} > 1, \quad \text{for } d/\text{SMD} > 0.8 \tag{5}$$

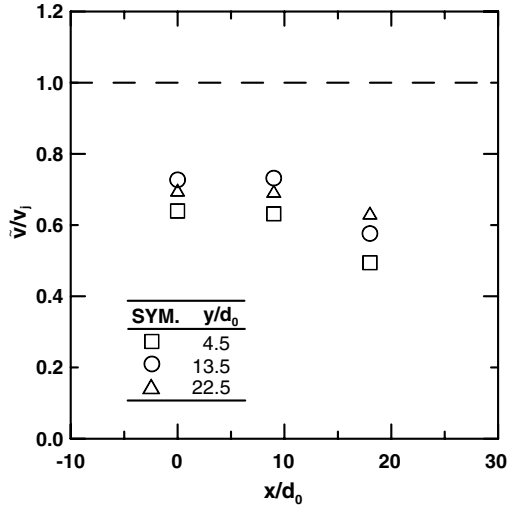

Fig. 17 Mass-averaged streamwise droplet velocities for different x/d_0 locations.

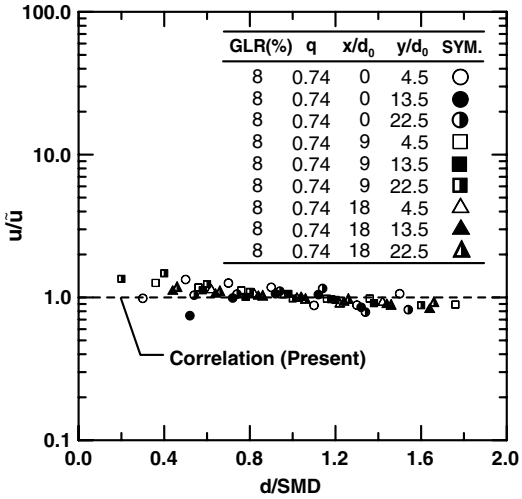

Fig. 18 Cross-stream droplets' velocity distribution normalized by mass-averaged cross-stream velocity as a function of droplet sizes.

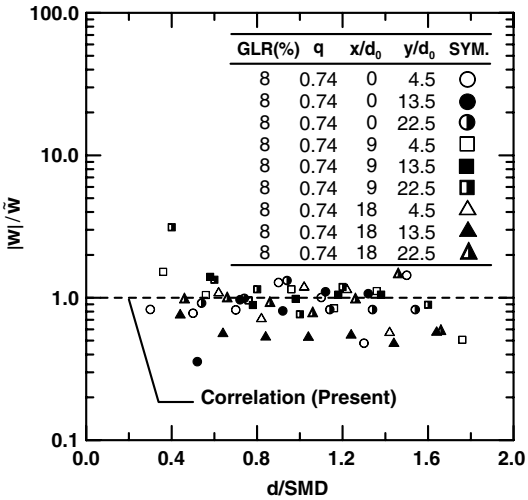

Fig. 20 Spanwise droplets' velocity distribution normalized by mass-averaged spanwise velocity as a function of droplet sizes.

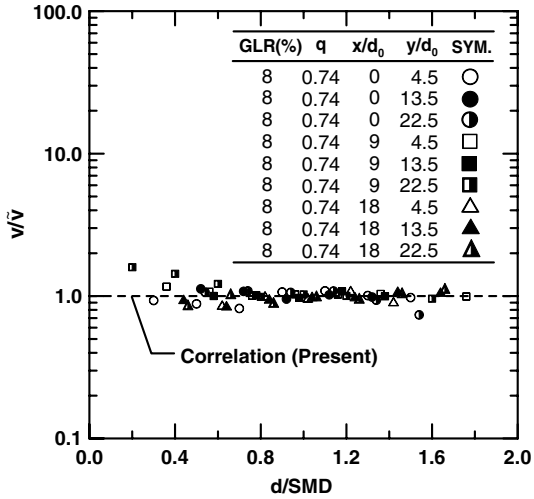

Fig. 19 Streamwise droplets' velocity distribution normalized by mass-averaged streamwise velocity as a function of droplet sizes.

$$u/\tilde{u} = 1, \quad \text{for } 0.8 < d/\text{SMD} < 1.2 \tag{6}$$

$$u/\tilde{u} < 1, \quad \text{for } d/\text{SMD} > 1.2 \tag{7}$$

The distribution of streamwise droplet velocities, v, normalized by the mass-averaged streamwise velocity, $\tilde{v}$, is shown in Fig. 19 as a function of droplet sizes normalized by the SMD. The streamwise droplet velocities, $v/\tilde{v}$, are unity for d/SMD greater than 0.4.

The magnitudes of the spanwise droplet velocities normalized by the magnitude of mass-averaged spanwise velocity, $\tilde{w}$, are shown in Fig. 20 as a function of droplet sizes normalized by the SMD. The spanwise droplet velocities were not influenced by d/SMD, unlike the streamwise and cross-stream velocities, probably due to the large uncertainties in the spanwise velocity measurements.

IV. Conclusions

The near-injector region ($x/d_0 = 0$–22.5, $y/d_0 = 0$–27) of aerated liquid jets in subsonic crossflow was investigated by double-pulsed DHM for the following test conditions: jet exit diameter of 1 mm, GLR = 8%, and momentum flux ratio of 0.74. The holograms were recorded on a CCD sensor with a spatial resolution of 5 mm and were numerically reconstructed at different spanwise distances. To overcome the limited field of view of DHM, the near-injector region has been divided into several investigation windows. To visualize the entire structure of the aerated liquid jet, a spray map was constructed by patching several reconstructed holograms with high resolution. Individual droplets' sizes, locations, and three-dimensional velocities were measured. Mass-averaged velocity distributions were obtained as functions of droplet sizes normalized by the SMD. The major conclusions of the present study are as follows:

1) Digital holographic microscopy is suitable for probing the dense-spray near-injector region for aerated liquid jets in subsonic crossflow. The present optical setup is relatively simple and does not require a collimating lens or relay lens unlike digital inline holography, which helps increase the resolution of the technique.

2) A large field of view can be obtained by simply patching several high resolution holograms reconstructed at the same spanwise distance.

3) Droplet velocities in three dimensions were measured by tracking their displacements during the time interval between the double pulses in the streamwise and cross-stream direction and by tracking the change in the plane of focus in the spanwise direction.

4) Most droplets in the probed region are nonspherical. The droplets were approximated as elliptical in shape and were characterized by their equivalent spherical diameter.

5) The distributions of the streamwise and cross-stream velocities were uniform in the near-injector region and could be characterized by the mass-averaged velocity except for very small and very large droplets.

6) The drop size distributions of aerated liquid jet in crossflow for the present test conditions (i.e., GLR 8%) followed Simmons's universal root-normal distribution (Simmons [13]) and thus could be fully described by the SMD alone.

Finally, the effort for the present manual processing of droplet velocities was large enough that there is a real need for automating the analysis of these digital holograms in the future to popularize this labor-intensive measuring technique.

Acknowledgments

Support from Taitech, Inc., under a subcontract with the U.S. Air Force Research Laboratory, is gratefully acknowledged. The initial development of experimental methods was carried out under the National Science Foundation grant EPS-0132534 (Oklahoma EPSCoR).

References

[1] Kim, J. Y., and Lee, S. Y., "Dependence of Spraying Performance on the Internal Flow Pattern in Effervescent Atomizers," *Atomization and Sprays*, Vol. 11, No. 6, 2001, pp. 735–756.

[2] Lefebvre, A. H., Wang, X. F., and Martin, C. A., "Spray Characteristics of Aerated-Liquid Pressure Atomizers," *Journal of Propulsion and*

Power, Vol. 4, 1988, pp. 293–298.
doi:10.2514/3.23066

[3] Buckner, H. N., and Sojka, P. E., "Effervescent Atomization of High-Viscosity Fluids: Part 1. Newtonian Liquids," *Atomization and Sprays*, Vol. 1, No. 3, 1991, pp. 239–252.

[4] Lund, M. T., Sojka, P. E., Lefebvre, A. H., and Gosselin, P. G., "Effervescent Atomization at Low Mass Flow Rates Part 1: The Influence of Surface Tension," *Atomization and Sprays*, Vol. 3, No. 1, 1993, pp. 77–89.

[5] Santangelo, P. J., and Sojka, P. E., "A Holographic Investigation of an Effervescent Atomizer-Produced Spray," *Atomization and Sprays*, Vol. 5, No. 2, 1995, pp. 137–155.

[6] Sutherland, J. J., Sojka, P. E., and Plesniak, M. W., "Entrainment by Ligament Controlled Effervescent Atomizer Produced Sprays," *International Journal of Multiphase Flow*, Vol. 23, 1997, pp. 865–884.
doi:10.1016/S0301-9322(96)00085-7

[7] Wade, R. A., Weerts, J. M., Sojka, P. E., Gore, J. P., and Eckerle, W. A., "Effervescent Atomization at Injection Pressures in the MPa Range," *Atomization and Sprays*, Vol. 9, No. 6, 1999, pp. 651–667.

[8] Lin, K.-C., Kennedy, P. J., and Jackson, T. A., "Spray Structures of Aerated-Liquid Jets in Subsonic Crossflows," AIAA Paper 2001-0330, 2001.

[9] Lin, K.-C., Kennedy, P. J., and Jackson, T. A., "Structures of Aerated Liquid Jets in High Speed Crossflows," AIAA Paper 2002-3178, 2002.

[10] Sallam, K. A., Aalburg, C., Faeth, G. M., Lin, K.-C., Carter, C. D., and Jackson, T. A., "Primary Breakup of Round Aerated-Liquid Jets in Supersonic Crossflows," *Atomization and Sprays*, Vol. 16, No. 6, 2006, pp. 657–672.
doi:10.1615/AtomizSpr.v16.i6.40

[11] Miller, B., Sallam, K. A., Bingabr, M., Lin, K.-C., and Carter, C. D., "Breakup of Aerated Liquid Jets in Subsonic Crossflow," *Journal of Propulsion and Power*, Vol. 24, No. 2, 2008, pp. 253–258.
doi:10.2514/1.30390

[12] Schnars, U., and Jueptner, W., *Digital Holography: Digital Hologram Recording, Numerical Reconstruction, and Related Techniques*, Springer, Berlin, 2005.

[13] Simmons, H. C., "Correlation of Drop-Size Distributions in Fuel Nozzle Sprays. 1. Drop-Size-Volume-Fraction Distribution," *Journal of Engineering for Power*, Vol. 99, No. 3, 1977, pp. 309–314.

T. Lieuwen
Associate Editor